Results in Physics 6 (2016) 1024–1030

Contents lists available at ScienceDirect

Results in Physics

journal homepage: www.journals.elsevier.com/results-in-physics

Fabrication and characterization of semiconductor nickel oxide (NiO) nanoparticles manufactured using a facile thermal treatment

Manal Hashem, Elias Saion, Naif Mohammed Al-Hada *, Halimah Mohamed Kamari, Abdul H. Shaari, Zainal Abidin Talib, Suriati B. Paiman, Mazliana A. Kamarudeen

Department of Physics, Faculty of Science, Universiti Putra Malaysia, 43400 Serdang, Selangor, Malaysia

ARTICLE INFO

Article history:
Received 2 November 2016
Received in revised form 16 November 2016
Accepted 16 November 2016
Available online 23 November 2016

Keywords:
Nanoparticles
Nickel oxide
Thermal treatment
Calcination
Optical properties

ABSTRACT

In this paper, thermal treatment procedures were utilised to prepare crystalline nickel oxide semiconductor nanoparticles, derived from an aqueous solution. The solution consists of three compounds, primarily nickel nitrate, polyvinyl pyrrolidine and deionised H_2O acting as metal precursor, capping agent and solvent, respectively. The solution was made prior to the drying, grinding and calcination at varying temperature settings up to 800 °C. The scanning Electron Microscopy (SEM) images allowed a detailed study on the morphological of the monocrystalline grains which were obviously observed in the specimen, showing them to be almost identical in shape and size. The Infrared Fourier Transform (FTIR) and X-ray diffraction (XRD) results demonstrated a transformation of the amorphous structure at room temperature to the crystalline structure at higher temperatures during calcination process. The mean particle diameter and particle distribution were found to be directly proportional to temperature increased. The transmission electron microscopic (TEM) analysis revealed that the particle diameters vary between 15 and 35 nm when temperature increased between 500 and 800 °C. The composition of the specimens was delineated by energy dispersed X-ray spectroscopy (EDX), which identified nickel and oxygen atomic percentages in the final products. Optical characteristics were deducted from a UV–Vis reflectance spectrophotometer, which demonstrated the energy band gap decrement as the calcination temperatures increased. Magnetic properties were determined through electron spin resonance spectroscopy (ESR), which revealed the presence of unpaired electrons. The magnetic field resonance decreases along with an increase of the g-factor value as the calcination temperature increased from 500 to 800 °C.

Introduction

In recently modern researches, metal and metal oxide nanoparticles have undergone a surge in interest as a result of their numerous physical/chemical properties, as well as their wider applicability over larger particle utilization [1,2]. As one example of these metal oxide nanomaterials, nickel oxide is a II–VI composite semiconductor made up of nickel (group II) and oxygen (group VI) from the periodic table of naturally elements [3]. The II-VI semiconductor NiO has a face centre cubic (fcc) crystal structure and is thought to be a material with many uses, as it demonstrates a range of intriguing chemical and physical characteristics. NiO is a P-type semiconductor transition metal oxide, which includes direct band gaps of 3.5–3.8 eV [4]. This unique structure results in a range of intriguing characteristics, which mean that NiO nanomaterials can be successfully employed in a range of physical applications

Nickel and its oxide nanoparticles show great potential for material use. They confer superior magnetic, electrical, thermal, optical, catalytic and mechanical performance [5–10]. Nickel oxide Nanostructures have been applied as catalysts, thermistors, sensors and additives, for gas and ceramic [11]. They are also found in battery electrodes and even stained glass [12–15] [5–8]. NiO nanoparticles are highly robust and feature a broad direct band gap of (3.56 eV). They are also p-type semiconductors and can be both super-paramagnetic and superanti-feromagnetic [16].

There are several approaches for synthesizing NiO crystalline nanoparticles which have been refined in recently published researches. Namely, via chemical reactive processes [17], electrodeposition [18], solution growth [14], pulsed-laser deposition [19], high-temperature nickel oxidation, spray pyrolysis [20], sputtering [21], sol–gel technique [22], the reverse-micellar route [23] and sol-gel formation [24]. Recently, the NiO nanoparticles have been synthesized using pulsed laser ablation technique then the

* Corresponding author.
E-mail address: naifalhada@yahoo.com (N.M. Al-Hada).

http://dx.doi.org/10.1016/j.rinp.2016.11.031
2211-3797/

structural and optical properties of the sample were investigated [25]. Spherical NiO nanoparticles were synthesized by microemulsion technique using rhamnolipids as the surfactant [26]. El-Kemary et al. synthesized NiO nanoparticles using the reaction of nickel chloride with hydrazine at room temperature and thermal decomposition of the $Ni(OH)_2$. It was reported that $Ni(OH)_2$ is calcinated at ~400 °C and obtained nanoparticles with size of 45 nm and the energy band gap of 3.54 eV [27]. Kumar et al. prepared Ni and NiO nanoparticles using water-in-oil microemulsions. The authors reported that NiO nanoparticles prepared by the reduction of $Ni(NO_3)_2$ with alkaline $NaBH_4$ using hydrazine hydrate as a reducing agent [28]. More recently, Fayem et al. synthesized NiO and PANI/NiO nanoparticles by using the precipitation technique [29]. Salavati-Niasari et al. synthesized NiO nanoparticles by heat-treatment of nickel octanoate $Ni(octa)_2$; (octa = octanoate); in the range of 400–900 °C. The authors have reported that the thermal treatment decomposition has some advantages such as simple process, low cost and easiness to obtain high purity products hence it is quite promising and facile route for industrial applications [7]. A further comparison between the present work and some of previous works has been shown in the Results and Discussion Section. But, the primary goals of some of the previously discussed works were to generate nanoscale materials which may be subject to fine manipulations – leading to inexpensive, eco-friendly and exceptionally pure for substances for many different usages in technology. Additionally, a lot of these methods are problematic given our present limited knowledge and the need for highly sophisticated methods in terms of long reaction durations, excessive temperatures and application of precursors which may be hazardous.

In this work, nickel oxide nanoparticles have been prepared via thermal treatment, utilizing only nickel nitrate, polyvinyl pyrrolidone and deionised H_2O as a precursor, capping agent and solvent, respectively, as per our prior research efforts [30–33]. The morphology and structure of the prepared NiO within the sample are ascertained though X-ray Spectroscopy (XRD) as well as Scanning and Transmission Electron Microscopy procedures (SEM/TEM). Optical specifications were derived through UV–Vis diffused reflectance spectrum. The Kubelka-Munk function used to ascertain the optical band gap energy. ESR (Electron Spin resonance spectroscopy) deduce magnetic properties of NiO nanoparticles in ambient temperatures. This approach is straight-forward, with inexpensive initial materials, and thus is a viable route for producing a large-scale product.

Experimental work

Materials

As discussed prior, the used materials were a nickel nitrate reagent, PVP and deionised H_2O. The polyvinyl pyrolidone, with a 58,000 g/mol molecular weight, was sourced from Sigma Aldrich. Nickel nitrate, the metal precursor, was purchased from Acros Organics with a molecular weight of 290.80 g/mol. No modifications were made upon receipt of these raw materials.

Synthesis of the nanoparticles

To produce the polymer solution, 4 g of PVP was added to 100 ml of H_2O (deionised). This was followed by the addition of 0.2 mmol of nickel nitrate $Ni(NO_3)_2{\cdot}6H_2O$. The solution was mixed for two hours in order to maximise homogeneity. H_2O was then evaporated by placing the solution in a petri dish and kept at 80 °C for twenty-four hours in an oven. The resultant solid was then ground with a pestle and mortar for fifteen minutes, separated into fifths and these were then each calcinated in incremental temperatures from 500 to 800 °C. The calcination process took place for three hours in order to form metal oxide crystallisation and the elimination of organic matter [31,34–37].

Characterisation

Several techniques were applied in order to ascertain the many properties of the formulated NiO crystalline particles. Structural properties were delineated via a Shimadzu model 6000 X-ray diffraction spectrometer (XRD), extrapolating 0.154 nm of CuKα as an aid for radiation which diffractive *S* from crystalline specimens at room temperature. Infrared measurements were taken via the Perkin Elmer 1650 FTIR (Fourier Transform Infrared Spectrometer) at 280–4000 cm^{-1}. Measurements also indicated the removal of the capping agents and organic compounds which result in the remaining NiO. Particle morphology, diameter, distribution and homogeneity were each measured by a JEOL 2010F UHR TEM model which ran at a 200 kV incremental speed voltage. Additionally, a Shimadzu UV-3600 UV–Vis spectrophotometer was utilised for ascertaining optical characteristics of specimens at ambient temperatures, ranging between 200 and 800 nm. Magnetic properties were deduced via an ESR machine in the same environment.

Results and discussion

Surface morphology

SEM analysis was performed to observe the morphological changes in the synthesized sample nanoparticles. The SEM micrographs of all the as-synthesized NiO nanoparticles at different calcination temperature are shown in Fig. 1. The surface morphological make-up of the NiO nanopowders having been calcinated between 500 and 800 °C was analysed by SEM. The resulting images are displayed in Fig. 1. The specimen comprised a consistently patterned NiO clusters in which collective sizes increased as temperatures rose. Rising of calcination temperatures results in amassed proximal clustering which are bounded to another and large in size [38].

FTIR study

FTIR reveals important elements concerning vibrational frequencies of functional groups, as well as their matrix structures. The preceding and resulting powder states after varied temperature treatments are shown in Fig. 2. FTIR specimens peak prior to the calcination temperature demonstrating substantial absorption of PVP polymer groupings. Absorption peaks of the following wave numbers 1649, 2938, 3408 cm^{-1} were paired with stretching vibration values of C═O, C—H, and N—H, in this order as Ansari et al. reported [37]. Peaks at 1427 cm^{-1} were paired to the C—H bending vibration sourced from the methylene group, whereas 1274 cm^{-1} linked to the stretching vibration value for C—N [31]. Lastly, 835 cm^{-1} linked to vibrations emergent in the C—C ring and 408 cm^{-1} to Ni—O. Temperatures of 500° and 600° generated bands of 1117 cm^{-1} and 1427 cm^{-1} and resulted from the basic hydrated carbonate banding vibrations. At the more extreme temperatures of 700 and 800 °C absorption peaks were isolated for NiO nanoparticles and were found to reduce in value as the temperature increased during the calcination procedure. This demonstrates that the NiO nanoparticles extrapolated from the process bestow exceptional purity. FTIR results conveyed nanoparticle and organic substance absorption bands are resultant from PVP degradation.

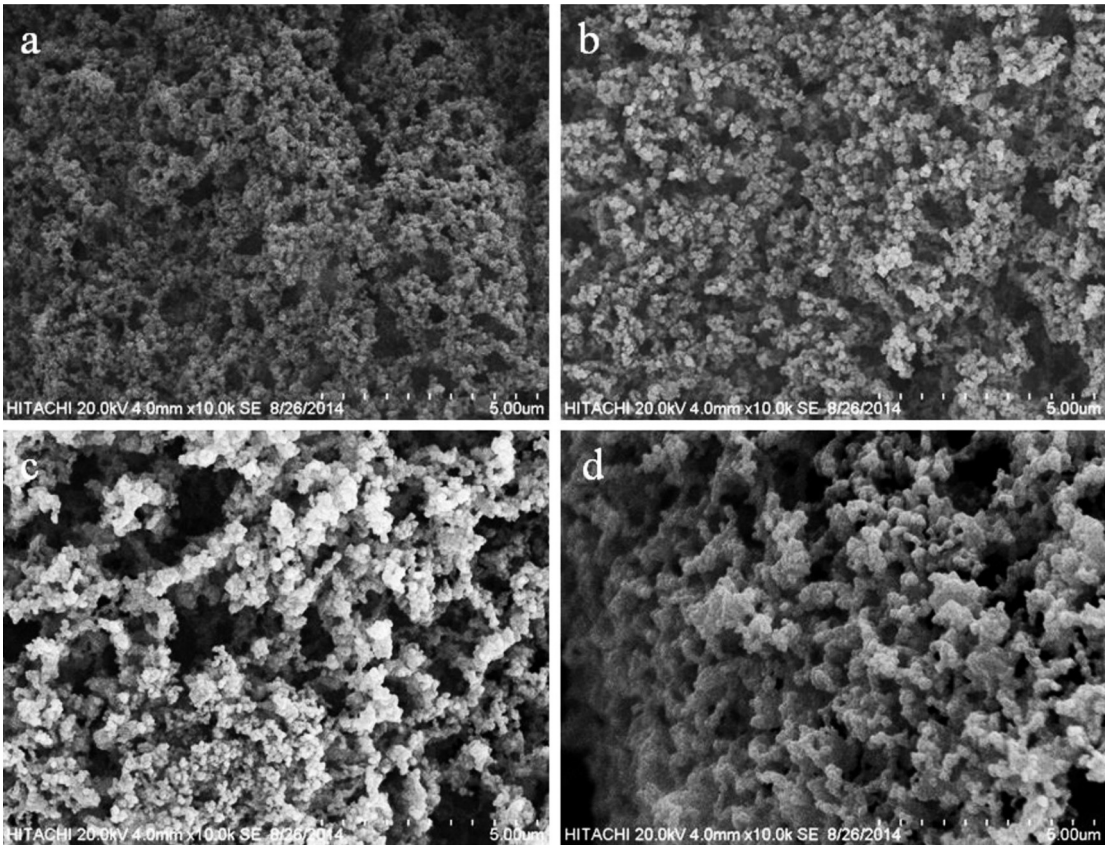

Fig. 1. SEM images of NiO nanoparticles at calcination temperatures of (a) 500 and (b) 600, (c) 700 and (d) 800 °C.

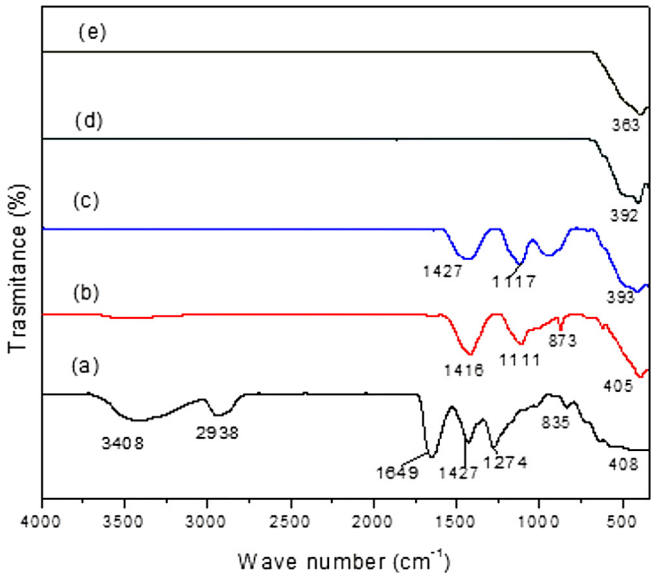

Fig. 2. FTIR spectra of (a) PVP and NiO nanoparticles at (a) 30, (b) 500, (c) 600, (d) 700, and (e) 800 °C in the range of 280–4500 cm^{-1}.

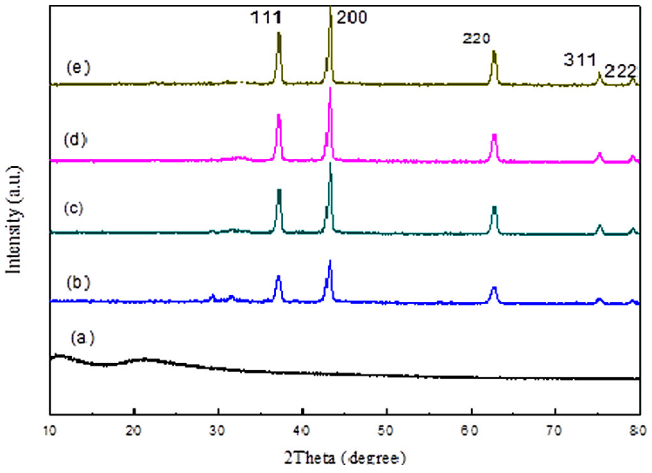

Fig. 3. XRD patterns of as-prepared and calcined NiO nanoparticles at different temperatures of (a) 30, (b) 500, (c) 600, (d) 700, and (e) 800 °C.

XRD

Powder X-ray diffraction (XRD), revealed crystalline parameters of the prepared NiO nanoparticle sample through a CuKα source wavelength of λ = 1.54056A°. Diffraction pattern of the powder was noted at a number of differing angles of diffraction (2θ) between 10° and 80°. Fig. 3 displays the X-ray diffraction patterning at the various calcination temperatures. Prior to the calcination process, it is suspected the specimen is in amorphous due to the absence of XRD peaks – only at 500 °C did they become apparent, indicative of the NiO nanoparticle structure in single phase. Regardless, crystallisation of NiO nanoparticles did not reach completion given the presence of nickel carbonate, evident from the peaks observed at 29° and 31°. However, the calcination process occurring at 600° did generate crystalline NiO nanoparticles of high purity and single phase in nature.

The presence of various diffractive peaks – (1 1 1), (2 0 0), (2 2 0), (3 1 1) and (2 2 2) planes within diffractive sequences indi-

cates the NiO specimens bestow an FCC structure (face centred cubic structure) as delineated by the JCPDS cards 36-1451. Decent crystalline conditions were obtained at >600°. Throughout the calcination process, peaks fluctuated, both increasing and decreasing in tandem as a result of optimal crystallinity conditions at 700° and 800°.

A growth in crystallinity means the constant expansion of the nanomaterial's overall mass throughout heating procedures to compensate interfacial surface energy. Diffractive peaks are suggested to be resultant of the NiO nanoparticles' cubic form.

Crystalline diameters were measured to be 14–34 nm following testing, and were deduced for the greatest peak magnitude of 2 0 0 through Scherrer's equation [39]. The results are listed thusly:

$$D = 0.9\lambda/\beta\cos\theta \quad (1)$$

where D is the crystallite size (nm), β is the full width of the diffraction line at half of the maximum intensity, i.e., (2 0 0) which is measured in radians, λ is the X-ray wave length of Cu Kα = 0.154 nm and θ is Bragg's angle [40].

X-ray diffraction patterns demonstrate the existence of powders manifested in their purest form, in single phase alignment and with no notable diffraction peaks aside from the typical peaks facilitated by the FCC phase NiO nanoparticles. As such it is evident that NiO nanoparticles that have been generated through the physical stages of preparation produce exceptional purity.

EDX

The EDX spectrum of NiO synthesis via thermal processes is presented in Fig. 4. Corresponding Ni and O peaks were found in the specimen, corroborating NiO nanoparticle synthesis and results generated by XRD measurements. The atomic percentage of Ni was 48.94%, with O constituting 51.06%. Peaks gold were derived from the initial stages of preparation for EDX observation. Additionally, heat treatment was found to be a highly efficient process given that the entire procedure evidently utilised all materials, resulting in no losses.

TEM

TEM provides diagnostics of size, distributes of differently sized particles and their agglomeration behaviour. Image J, a specialised computer program, was used to measure particle sizes and their distribution, by means of taking specimens with >100 nanoparticles each. Fig. 5 is a histogram that demonstrates the relevant particle size and their distributes, for each of the different calcination temperature settings. Additionally, it shows that NiO nanoparticles derived from the process are spherical, with small distribution sizes. Calcination temperature (ranging from 500 to 800 °C) and particle size were found to be directly proportionate [34,35]. This is indicative of PVP degradation through temperature increase, which in turn triggers proximal particles to bind, resulting in an overall increased mass [30,36,41]. In the context of 500 °C heat treatment, 15 nm was a typical measurement; this figure increased to 35 nm in 800 °C the treatment context, which further corroborates XRD findings (listed in Table 1) relating to particle size measurements.

Optical properties

Optical Diffuse Reflectance Spectra (DRS) were recorded via UV–Vis spectroscopy for the NiO nanoparticles. An energy band gap is depicted in Fig. 6 for nanoparticles analysed through the DRS, the following was obtained in using the Kubelka-Munk function, given in Eq. (2):

$$(F(R\infty)\cdot h\nu)^2 = (A\cdot(h\nu\text{-}Eg)) \quad (2)$$

here, F(R∞) is the "emission parameter", or Kubelka-Munk function, $h\nu$ represents incident photon energy, A is a constant, dependent on both transition likelihood and the diffuse reflectance R∞, and R∞ is the diffuse reflectance derived from R∞ = Rsample/Rstandard [42]. In plotting the square provided by the Kubelka Munk function $[F(R)\ h\nu]^2$ vs. energy, and by elucidating the linear aspect of the curve to $[F(R)h\nu]^2 = 0$ for the specimens having undergone calcination at temperatures between 500 and 800 °C, the direct band gap energy of the substance may be obtained. Optical band gaps of 3.60, 3.57, 3.55, and 3.51 eV were ascertained for specimens having undergone calcination at 500, 600, 700 and 800 °C, in this order, demonstrated by Table 1. Values of energy band gap were found to be inversely proportionate to the calcination temperature increases as a result of quantum size phenomena. If a nanoparticle produces energy band composure, then if the quantity of atoms were to rise, electronic bands within the particle will be drawn to the core as a result of an increase in protons [43]. A com-

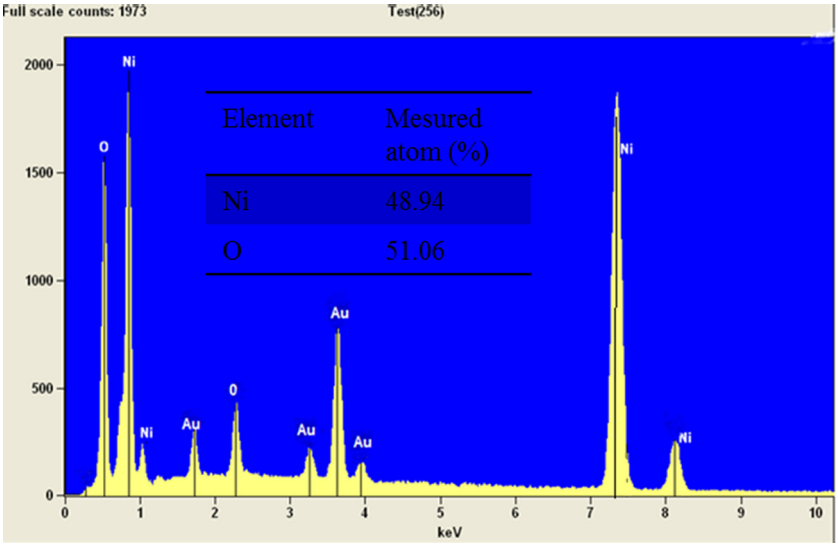

Fig. 4. The EDX spectrum of the NiO nanoparticles calcined at 700 °C.

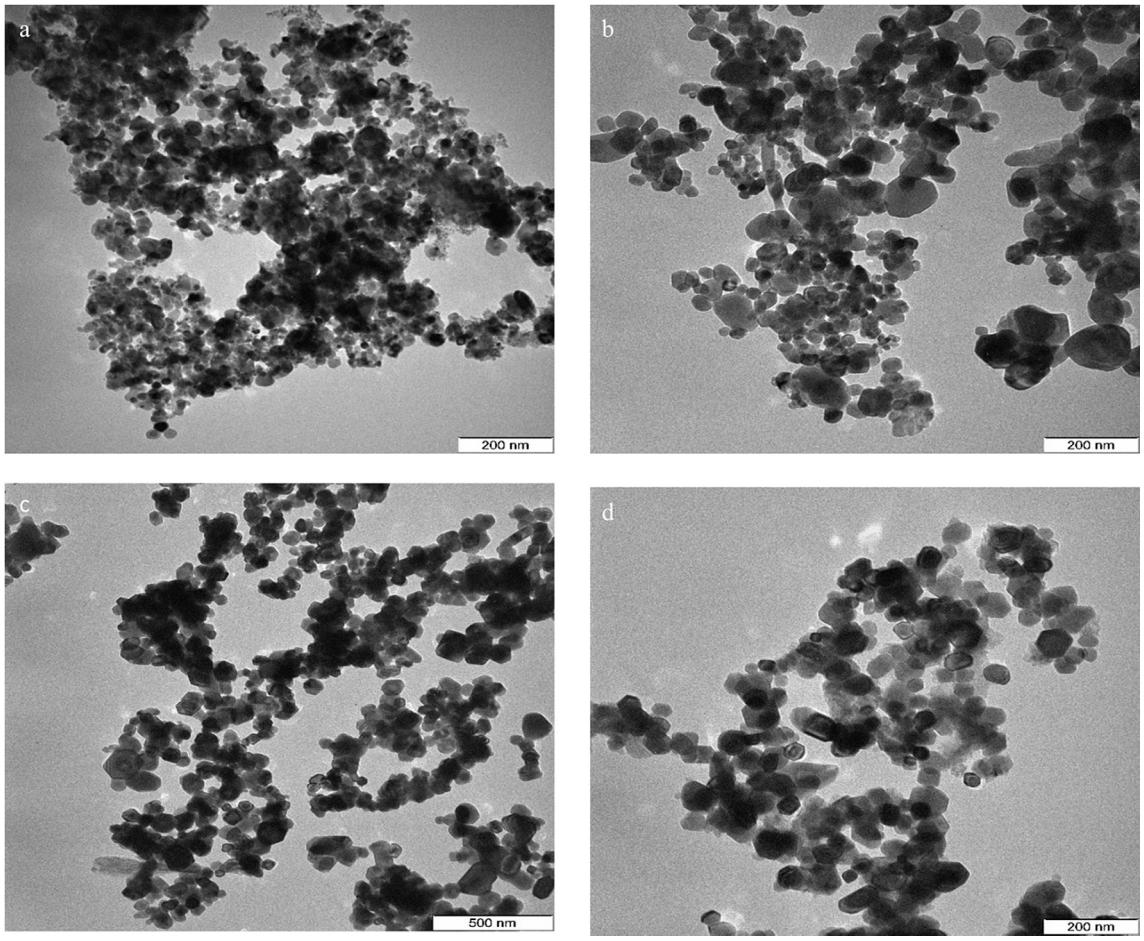

Fig. 5. TEM images and particle size distribution of NiO nanoparticles at calcination temperature of (a) 500, (b) 600, (c) 700 and (d) 800 °C.

Table 1
Summary of the structural and optical properties of synthesized NiO nanoparticles at different calcination temperatures.

Temperature (°C)	D_{XRD} (nm)	D_{TEM} (nm)	Eg (eV)
500	14	15 ± 4	3.60
600	19	20 ± 2	3.57
700	21	23 ± 3	3.55
800	34	35 ± 3	3.51

parison between the present work and some of previous works has been shown in Table 3.

Electron spin resonance

The electron spin resonance spectrum (ESR) for the various calcination temperature iterations is given in Fig. 7. Results appear to have wide scope and are symmetrical, as a result of unpaired elec-

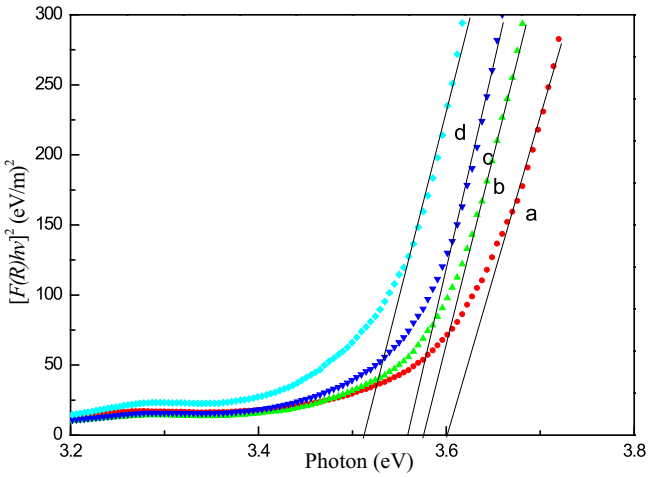

Fig. 6. The method of extracting the band gaps of NiO nanoparticles calcined at different temperatures of (a) 500, (b) 600, (c) 700 and (d) 800 °C.

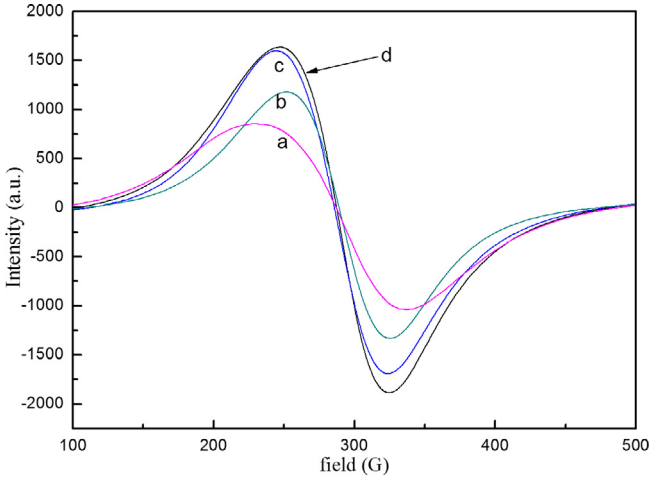

Fig. 7. ESR spectra of NiO nanoparticles calcined at different temperatures of (a) 500, (b) 600, (c) 700 and (d) 800 °C.

trons from conduction electrons of transition Ni^{2+} ions; these were all found in the specimens of the various temperature environments to suggest paramagnetic characteristics. A decrease in the overall resonant magnetic field was observed between 296.4 and 289.7 G as temperatures of the calcination processes increased between 500 and 800 °C, as presented in Table 2. The table also shows a rise in g-factor from 2.28167 to 2.29367 across the calcination temperature variations. This is suggestive of the fact that the inner-magnetic field rose as the calcination temperatures increased, meaning that generally, magnetic properties are magnified as particle size rises. The *g*-factor value is provided through means of the following equation:

$$g = (h\upsilon)/(\beta\, Hr) \quad (3)$$

Here, h = Planck's constant, υ represents microwave frequency, and β = Bohr magneton ($9.274 \times 10{-}24\ J{\cdot}T^{-1}$). *Hr* represents the resonant magnetic field; this value is expected to fall in the case of a rise in g-factor. However, υ values are constants according to EPR Spectroscopy analysis. Rises in g-factor, reduction of Hr, and subsequently increases in magnetisation have been established in prior research concerning NiO nanoparticles.

Table 2
Magnetic parameters of NiO nanoparticles observed for ESR analysis.

Temperature (°C)	?? factor	*Hr* (Oe)
500	2.28167	296.4
600	2.28343	294.2
700	2.29307	291.9
800	2.29367	289.7

Table 3
A comparison between the present work and some of previous works.

Method	Size (nm)	Energy band gap (eV)	References
Pulsed laser ablation	8	3.62	Gondal et al. [25]
Thermal decomposition	45	3.54	El-Kemary, et al. [27]
Microemulsions	8–100	–	Kumar et al. [28]
Precipitation	40	~3.64	Fayem et al. [29]
Emulsion	47	–	Palanisamy and Raichur [26]
This method	14–35	3.51–3.60	

Formation mechanism of the NiO nanoparticles

In Fig. 8, the interaction between the Ni ions and PVP prior to the calcination procedure is suggested. Ni $(NO_3)_2$ was combined with PVP as agent and H_2O acting as the solvent. As the solution is mixed, metallic ions attract amine groups of polymer chains via ionic-dipole communication. Following this, a "mobility congealment" of metallic cations within the polymer depression was implemented, resulting from the absence of H_2O in the dry solution. The gradual disappearance of PVP throughout the calcination procedure and increased temperatures facilitate the formation and development of NiO nanoparticles, which then cause proximal particles to bind together. Once the calcination process was complete, PVP values and unnecessary anions were eliminated from the specimen, as NiO nanoparticles form, combine, and exceed interfacial surface energy. Thus, they amass into larger particles, the greater the temperature, the larger the resultant particles. It is here hypothesised that PVP is instrumental in NiO nanoparticle nucleation, as well as its role as a manipulative tool to yield desired particle sizes [30,31,33].

Conclusions

In this study, NiO nanoparticles have been produced through a basic heat treatment procedure. Particles ranging from 15 to 35 nm in size were obtained through the varying thermal treatment which ranged from 500 to 800 °C, with smaller sizes yielded at lower temperatures. Many tools have been utilised in ascertaining the many nanoparticle properties, namely, FTIR spectroscopy, which delineated NiO bands for all contexts. Ni and O peaks were derived via EDX analysis, which showed that NiO indeed formed following calcination procedures. The Kubelka-Munk function revealed from UV–vis reflectance spectra that the band gap energy

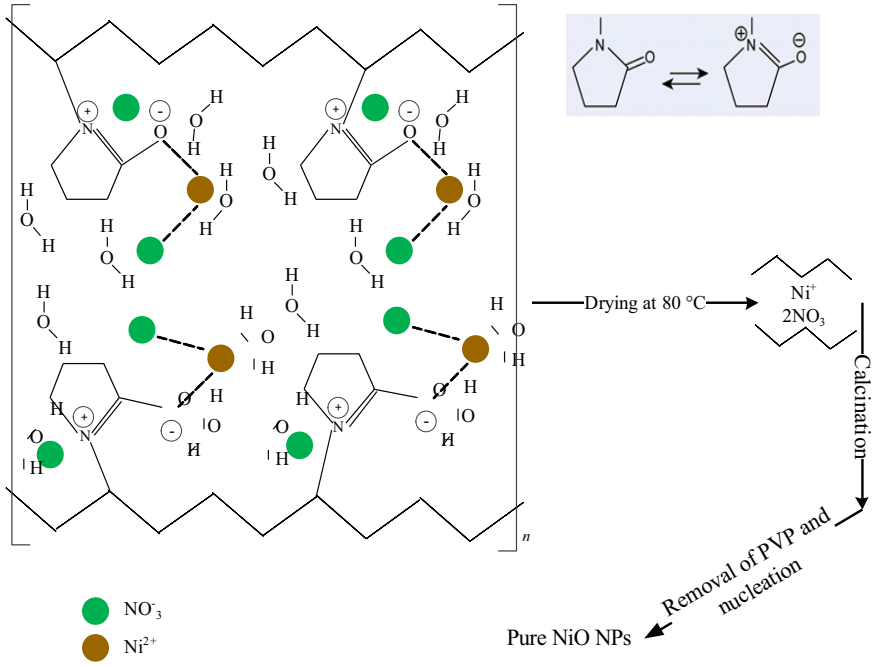

Fig. 8. A proposed mechanism of the interaction between PVP and metallic ions [30].

value of NiO was predicted to decline from 3.60 to 3.51 eV as calcination temperatures rose from 500 to 800 °C, respectively. ESR spectroscopy revealed the presence of unpaired electrons, with *Hr* and *g*-factors also delineated. Rises in *g*-factor and decline in the RMF, *Hr*, followed the incremental increase in calcination temperatures from 500 to 800 °C. This suggests an increase in the magnetic potency of the observed specimens, in which particle size rose proportional with calcination temperatures.

Conflicts of interest

The authors declare no conflict of interest.

Acknowledgment

The authors would like to thank staff of Universiti Putra Malaysia for the assistance received in completion of this work.

References

[1] Li Q, Wang L-S, Hu B-Y, Yang C, Zhou L, Zhang L. Mater Lett 2007;61:1615–8.
[2] Xin X, Lü Z, Zhou B, Huang X, Zhu R, Sha X, Zhang Y, Su W. J Alloy Compd 2007;427:251–5.
[3] Palombari R. J Electroanal Chem 2003;546:23–8.
[4] Ai L, Fang G, Yuan L, Liu N, Wang M, Li C, Zhang Q, Li J, Zhao X. Appl Surf Sci 2008;254:2401–5.
[5] Aricò AS, Bruce P, Scrosati B, Tarascon J-M, Van Schalkwijk W. Nat Mater 2005;4:366–77.
[6] Siegel RW. Nanostructure science and technology: R & D status and trends in nanoparticles, nanostructured materials and nanodevices. Springer; 1999.
[7] Salavati-Niasari M, Davar F, Fereshteh Z. J Alloy Compd 2010;494:410–4.
[8] Ansari F, Bazarganipour M, Salavati-Niasari M. Mater Sci Semicond Process 2016;43:34–40.
[9] Salavati-Niasari M, Mohandes F, Davar F, Mazaheri M, Monemzadeh M, Yavarinia N. Inorg Chim Acta 2009;362:3691–7.
[10] Salavati-Niasari M, Mir N, Davar F. Polyhedron 2009;28:1111–4.
[11] Zhao L, Su G, Liu W, Cao L, Wang J, Dong Z, Song M. Appl Surf Sci 2011;257:3974–9.
[12] Chen F, Liu M. J Mater Chem 2000;10:2603–5.
[13] Miller EL, Rocheleau RE. J Electrochem Soc 1997;144:3072–7.
[14] Pejova B, Kocareva T, Najdoski M, Grozdanov I. Appl Surf Sci 2000;165:271–8.
[15] Yoshio M, Todorov Y, Yamato K, Noguchi H, Itoh J-I, Okada M, Mouri T. J Power Sources 1998;74:46–53.
[16] Kodama RH, Makhlouf SA, Berkowitz AE. Phys Rev Lett 1997;79:1393.
[17] Kumagai H, Matsumoto M, Toyoda K, Obara M. J Mater Sci Lett 1996;15:1081–3.
[18] Varkey AJ, Fort AF. Thin Solid Films 1993;235:47–50.
[19] Fasaki I, Giannoudakos A, Stamataki M, Kompitsas M, György E, Mihailescu I, Roubani-Kalantzopoulou F, Lagoyannis A, Harissopulos S. Appl Phys A 2008;91:487–92.
[20] Patil P, Kadam L. Appl Surf Sci 2002;199:211–21.
[21] Estrada W, Andersson AM, Granqvist CG. J Appl Phys 1988;64:3678–83.
[22] Danial AS, Saleh MM, Salih SA, Awad MI. J Power Sources 2015;293:101–8.
[23] Ahmad T, Ramanujachary KV, Lofland SE, Ganguli AK. Solid State Sci. 2006;8:425–30.
[24] Nalage S, Chougule M, Sen S, Joshi P, Patil V. Thin Solid Films 2012;520:4835–40.
[25] Gondal MA, Saleh TA, Drmosh QA. Appl Surf Sci 2012;258:6982–6.
[26] Palanisamy P, Raichur AM. Mater Sci Eng C 2009;29:199–204.
[27] El-Kemary M, Nagy N, El-Mehasseb I. Mater Sci Semicond Process 2013;16:1747–52.
[28] Kumar A, Saxena A, De A, Shankar R, Mozumdar S. Adv Nat Sci: Nanosci Nanotechnol 2013;4:025009.
[29] Fayemi OE, Adekunle AS, Ebenso EE. J Nanomater 2016;2016.
[30] Al-Hada NM, Saion EB, Shaari AH, Kamarudin MA, Flaifel MH, Ahmad SH, Gene SA. PLoS ONE 2014;9:e103134.
[31] Al-Hada NM, Saion EB, Shaari AH, Kamarudin MA, Flaifel MH, Ahmad SH, Gene A. Mater Sci Semicond Process 2014;26:460–6.
[32] Al-Hada NM, Saion E, Kamari HM, Flaifel MH, Shaari AH, Talib ZA, Abdullahi N, Baqer AA, Kharazmi A. Mater Sci Semicond Process 2016;53:56–65.
[33] Al-Hada NM, Saion E, Talib ZA, Shaari AH. Polymers 2016;8:113.
[34] Ghanbari D, Salavati-Niasari M, Sabet M. Compos B Eng 2013;45:550–5.
[35] Ansari F, Sobhani A, Salavati-Niasari M. J Magn Magn Mater 2016;401:362–9.
[36] Ansari F, Sobhani A, Salavati-Niasari M. RSC Adv 2014;4:63946–50.
[37] Ansari F, Soofivand F, Salavati-Niasari M. Mater Charact 2015;103:11–7.
[38] Dharmaraj N, Prabu P, Nagarajan S, Kim CH, Park JH, Kim HY. Mater Sci Eng B 2006;128:111–4.
[39] Cullity BD, Stock SR. Elements of X-ray diffraction. Pearson; 2001.
[40] Klug HP, Alexander LE. In Harold P Klug, Leroy E Alexander (Eds.), X-ray diffraction procedures: for polycrystalline and amorphous materials, 2nd ed. Wiley-VCH; 1974. p. 992. ISBN 0-471-49369-4.
[41] Gene SA, Saion E, Shaari AH, Kamarudin MA, Al-Hada NM, Kharazmi A. J Nanomater 2014;2014:1–7.
[42] Torrent J, Barron V. Encyclopedia of surface and colloid science. New York: Marcel Dekker Inc.; 2002.
[43] Gharibshahi E, Saion E. Int J Mol Sci 2012;13:14723–41.